

PAPER: Disordered systems, classical and quantum

Multiscaling in the 3D critical site-diluted Ising ferromagnet

E Marinari¹, V Martin-Mayor², G Parisi¹,
F Ricci-Tersenghi^{1,*} and J J Ruiz-Lorenzo³

¹ Dipartimento di Fisica, Sapienza Università di Roma and CNR-Nanotec, Rome unit, and INFN, Sezione di Roma, I-00185 Rome, Italy

² Departamento de Física Teórica, Universidad Complutense, 28040 Madrid, Spain

³ Departamento de Física and Instituto de Computación Científica Avanzada (ICCAEx), Universidad de Extremadura, 06006 Badajoz, Spain

E-mail: federico.ricci@uniroma1.it

Received 14 September 2023

Accepted for publication 25 November 2023

Published 12 January 2024



Online at stacks.iop.org/JSTAT/2024/013301

<https://doi.org/10.1088/1742-5468/ad13fe>

Abstract. We study numerically the appearance of multiscaling behavior in the 3D ferromagnetic Ising site-diluted model, in the form of a multifractal distribution of the decay exponents for the spatial correlation functions at the critical temperature. We have computed the exponents of the long-distance decay of higher moments of the correlation function, up to the 10th power, by studying three different quantities: global susceptibilities, local susceptibilities and correlation functions. We have found very clear evidence of multiscaling behavior.

Keywords: multifractality at critical points of disordered systems

* Author to whom any correspondence should be addressed.



Original Content from this work may be used under the terms of the [Creative Commons Attribution 4.0 licence](https://creativecommons.org/licenses/by/4.0/). Any further distribution of this work must maintain attribution to the author(s) and the title of the work, journal citation and DOI.

Contents

1. Introduction	2
2. Model, simulations and observables	4
2.1. The model	4
2.2. Our numerical simulations	4
2.3. Definition of main observables	4
2.3.1. Correlations.	4
2.3.2. Global susceptibilities.	5
2.3.3. Local susceptibilities.	6
2.4. Details of the computation of the observables	6
2.4.1. The computation of χ_q	7
2.4.2. The computation of $\tilde{\chi}_q$	8
2.4.3. The computation of $C_q(r)$	8
3. Numerical results	9
3.1. Correlation functions	9
3.2. Global susceptibilities	10
3.3. Local susceptibilities	12
4. Discussion and conclusion	14
Acknowledgments	15
Appendix. Some theoretical results	16
A.1. Scaling dimensions	16
A.2. Concavity of the scaling exponents	17
A.3. Davis–Cardy’s result	17
References	18

1. Introduction

The extension of statistical mechanics to the study of systems with quenched disorder is of paramount importance. Much effort has been devoted to this task in recent decades, and much important information has been established. Here, universality is the key. For pure systems, critical exponents take a few values that only depend on crucial features of the system, such as its dimensionality, the nature of its fields and the symmetries of the Hamiltonian. How this idea extends to the system where the Hamiltonian is characterized by quenched disorder has been discussed at length and is still, at least partially, an open problem.

The diluted ferromagnetic Ising model (denoted as DIM hereafter) is one of the crucial prototypes on which the entrance of quenched disorder in statistical mechanics is analyzed. Here, even an infinitesimal amount of dilution (that can be a site or a link dilution, leading to models showing basically the same physical behavior) in a pure model, with a positive specific heat critical exponent, will change the universality class and the critical exponents [1, 2].

Here, in order to further clarify crucial properties of the DIM, we consider the behavior of correlation functions and of susceptibilities. At a second order phase transition, the correlation length ξ diverges at the critical point T_c when the volume V of the system diverges. When the position of the critical point is known, we can analyze correlation functions C there, where they are expected to scale as a power law of the distance, with an exponent, say, τ . A usual scaling law would suggest that the q th moment of the correlation function $C(r)$ would scale with an exponent $\tau(q)$ equal to $q\tau(1)$ (see later for details and precise definitions).

We find here that in a 3D, $D = 3$ diluted Ising model, this is not true, and we get what is called *multi-fractal* behavior [3, 4]. We determine with high accuracy the values of these exponents, and show numerically that they do not obey the relation $\tau(q) = q\tau(1)$.

The multiscaling behavior of the correlation functions has been thoroughly studied in the context of 2D ferromagnetic spin models with quenched disorder (Potts models with more than two states and site or link dilution) using conformal field techniques and numerical simulations [5–11]. In another context, we can also quote the multiscaling behavior that appears in the strong-amplitude fluctuations of the wave functions in the Anderson localization [12].

To achieve such a result in a 3D ‘simple’ disordered system (simple as opposed to spin glasses, where the same fact has been recently established numerically for all values of the temperature in the broken phase [13]) is in some sense unexpected. However, indeed some important theoretical results achieved by Davis and Cardy, many years ago, have clarified the plausibility of this fact [14, 15]. Conformal invariance allows crucial developments in critical scaling, starting from 2D systems [5]. By applying to this context the renormalization group and an ε expansion, Davis and Cardy were able to show that in the DIM one expects multifractality in $2 + \varepsilon$ dimensions [15].

Our numerical findings, which we support with theoretical arguments, are consistent with Davis and Cardy’s computation [15] (see also A.3). As many results in the field explain, there are indeed many factors that have to be considered. Logarithmic corrections also appear in these kinds of contexts, and we have been able to use numerics to clearly show that in this case we are observing a real, bona fide multifractality. We will discuss this in detail in the following.

The structure of the paper is as follows. We first define our model (section 2.1), describe the numerical approach we follow (section 2.2), define the observable quantities that we compute (section 2.3) and then explain how we compute these quantities (section 2.4). Next, we show our numerical results in section 3. Finally, we discuss our results and draw some conclusions in section 4. The paper is complemented with an appendix, where we remind the reader of relevant theoretical results.

2. Model, simulations and observables

2.1. The model

We have considered the $D = 3$ diluted Ising model defined on a cubic lattice with periodic boundary conditions, linear size L and volume $V = L^D$. The Hamiltonian of the model, in zero magnetic field, has the form,

$$\mathcal{H} = - \sum_{\langle x,y \rangle} \epsilon_x \epsilon_y s_x s_y, \quad (1)$$

where s_x are Ising variables and ϵ_x are statistically independent quenched random variables, which take the value 1 with probability p and the value 0 with probability $1 - p$. A set of $\{\epsilon_x\}$ defines a *sample*. The sum in equation (1) runs over all pairs of lattice nearest-neighbors. As usual, we denote with $\langle(\dots)\rangle$ the thermal average for the $\{s_x\}$, which is computed for a *fixed* set of disorder variables $\{\epsilon_x\}$. The average over the samples, $\overline{(\dots)}$, is only taken after thermal mean values have been computed for each sample.

2.2. Our numerical simulations

We have investigated the model defined in equation (1) through equilibrium numerical simulations. Specifically, we have brought our samples to thermal equilibrium by combining Wolff's single-cluster algorithm [16], with a local Metropolis method. The remarkable effectiveness of this combination of simulation algorithms in DIM simulations was demonstrated long ago [17, 18]. Specifically, our elementary Monte Carlo steps consisted on L single-cluster updates, followed by a sequential full-lattice Metropolis update.

In particular, we have fixed the (average) spin density to $p = 0.8$, because for this value the scaling corrections are very small, even negligible, given our statistical errors. The model is almost governed by a *perfect action* [18, 19]. Furthermore, we have performed all our simulations at the infinite volume critical inverse temperature [19]: $\beta_c^{(p=0.8)} = 0.2857429(4)$. For future use, we note that the anomalous dimension of the field is $\eta = 0.036(1)$ [19]. Further details of our simulations can be found in table 1.

2.3. Definition of main observables

In the next three paragraphs we describe the different observables used to analyze the multiscaling properties of our model (1).

2.3.1. Correlations. The relevant correlation functions are,

$$C_q(r) = \frac{1}{pV} \sum_x \overline{\langle \epsilon_x s_x \epsilon_{x+r} s_{x+r} \rangle^q}. \quad (2)$$

As usual, we assume that rotational invariance is recovered in the scaling limit $\xi \gg 1$, and we indicate only the dependence of $C_q(r)$ on the length r of the displacement vector \mathbf{r} .

In order to study multiscaling behavior, we introduce the $\zeta(q)$ and $\tau(q)$ exponents through the following relations:

$$C_q(r) \sim \frac{1}{r^{\tau(q)}} \sim [C_1(r)]^{\zeta(q)}. \quad (3)$$

It follows that $\tau(q)$ and $\zeta(q)$ are connected by the relation,

$$\tau(q) = (D - 2 + \eta)\zeta(q), \quad (4)$$

because,

$$C_1(r) \sim \frac{1}{r^{D-2+\eta}}. \quad (5)$$

By definition, $\zeta(1) = 1$ and $\tau(1) = D - 2 + \eta$. In the absence of multiscaling behavior one would have $\tau(q) = (D - 2 + \eta)q$ or, equivalently, $\zeta(q) = q$ (see A.1 for more details). Instead, we find that $\zeta(q) < q$ whenever $q > 1$.

Finally, in order to compute the ζ exponent, minimizing the scaling corrections, we analyze the ratio:

$$\frac{C_q}{C_1^q} \sim [C_1]^{\zeta(q)-q}. \quad (6)$$

2.3.2. Global susceptibilities. We define the χ_q susceptibilities as,

$$\chi_q = \frac{1}{pV} \sum_{xy} \overline{\langle \epsilon_x s_x \epsilon_y s_y \rangle^q}, \quad (7)$$

which scale with L as,

$$\chi_q \sim \int^L d^D x C_q(r) \sim L^{D-\tau(q)}, \quad (8)$$

provided that $D > \tau(q)$. The above relation allows us to compute $\tau(q)$ and, from it, $\zeta(q)$. If $D < \tau(q)$, we have that,

$$\chi_q \sim L^0. \quad (9)$$

Equations (8) and (9) provide a very direct test for multiscaling. Indeed, given that $\tau(1) = 1.036(1)$ in 3D, one notes that $q\tau(1) > D$ whenever $q \geq 3$. Hence, finding (as we do below) that $\chi_{q=3}$ scales with a positive power of L gives a direct confirmation of the multiscaling behavior.

2.3.3. *Local susceptibilities.* Another strategy is based on computing a different ‘local susceptibility’ $\tilde{\chi}_q$ defined as,

$$\tilde{\chi}_q = \frac{1}{pV} \sum_x \overline{\chi_x^q}, \quad (10)$$

with,

$$\chi_x = \sum_y \langle \epsilon_x s_x \epsilon_y s_y \rangle. \quad (11)$$

The scaling of this observable, see A.1, is such that,

$$R_q^{(1)} \equiv \frac{\tilde{\chi}_q}{\tilde{\chi}_1^q} \sim L^{(D-2+\eta)(q-\zeta(q))/2}. \quad (12)$$

Note that $\tilde{\chi}_1 = \chi_1$.

We are able to compute numerically the first two derivatives of $\zeta(q)$ by computing ($q \geq 2$):

$$R_q^{(2)} \equiv \frac{\tilde{\chi}_q}{\tilde{\chi}_{q-1}} \sim L^{(D-2+\eta)(\zeta(q-1)-\zeta(q))/2} \quad (13)$$

and (for the discrete proxy of the second derivative),

$$R_q^{(3)} \equiv \frac{\tilde{\chi}_q \tilde{\chi}_{q-2}}{\tilde{\chi}_{q-1}^2} \sim L^{(D-2+\eta)(2\zeta(q-1)-\zeta(q)-\zeta(q-2))/2}. \quad (14)$$

2.4. Details of the computation of the observables

Since the computation of the correlation function $C_q(r)$ technically differs from the computation of the global susceptibility χ_q (that, on its side, is also very different to the computation of the local susceptibility $\tilde{\chi}_q$), we have chosen to discuss these points in separate sections.

For the computation of χ_q and $\tilde{\chi}_q$ we shall be employing *real replicas* for each sample. Real replicas are statistically independent system copies that evolve under the same quenched disorder $\{\epsilon_x\}$.

Furthermore, our computation of the two susceptibilities uses the enhanced cluster estimator [20]:

$$\langle \epsilon_x s_x \epsilon_y s_y \rangle = \langle \gamma_{y,x} \rangle, \quad (15)$$

where $\gamma_{y,x} = 1$ if, and only if,

- $\epsilon_x = \epsilon_y = 1$,

- When the lattice is decomposed on Fortuin–Kasteleyn clusters, both sites \mathbf{x} and \mathbf{y} happen to belong to the same cluster.

Otherwise, $\gamma_{\mathbf{y},\mathbf{x}} = 0$.

2.4.1. The computation of χ_q . Our computation of the global susceptibilities χ_q uses 12 real replicas. Let $\gamma_{\mathbf{y},\mathbf{x}}^{(a)}$ be the enhanced estimator for correlation functions obtained from replica a , ($a = 1, 2, \dots, 12$).

Our estimator of χ_q is obtained in the following way. We start by randomly choosing a starting site \mathbf{x} and trace the cluster to which \mathbf{x} belongs in all 12 replicas. Next, we select a set of q distinct replicas a_1, a_2, \dots, a_q , and compute,

$$M_{\mathbf{x}}^{(q)} = \sum_{\mathbf{y}} \left(\prod_{j=1}^q \gamma_{\mathbf{y},\mathbf{x}}^{(a_j)} \right). \quad (16)$$

Defining the number of spins as,

$$N_{\text{spins}} = \sum_{\mathbf{x}} \epsilon_{\mathbf{x}}, \quad (17)$$

one easily finds that,

$$\frac{1}{N_{\text{spins}}} \sum_{\mathbf{x}} \langle M_{\mathbf{x}}^{(q)} \rangle = \frac{1}{N_{\text{spins}}} \sum_{\mathbf{xy}} \overline{\langle \epsilon_{\mathbf{x}} s_{\mathbf{x}} \epsilon_{\mathbf{y}} s_{\mathbf{y}} \rangle^q}. \quad (18)$$

Of course, in order to improve the statistical accuracy, one can average over different choices of a subset of q distinct replica indices. Note that in practice we choose just one starting site \mathbf{x} in equation (18). The starting site is chosen with uniform probability $1/N_{\text{spins}}$.

Now, given that,

$$\overline{N_{\text{spins}}} = pV, \quad (19)$$

and that the fluctuations of N_{spins} do not play any relevant role⁴, we may approximate,

$$\chi_q \approx \overline{\langle M_{\mathbf{x}}^{(q)} \rangle}. \quad (20)$$

A final note of warning is in order. In the update of the spin configuration, we cannot employ the same Fortuin–Kasteleyn clusters that we employ in the computation of the

⁴ More quantitatively, trading $1/pV$ with $1/N_{\text{spins}}$ only induces additional corrections to scaling, of size L^{-a} with $a = D - \frac{1}{\nu} \geq D/2$. This estimate can be obtained by combining the following three observations: (i) $\overline{(N_{\text{spins}} - pV)\langle O \rangle} = p(1-p)\frac{\partial \langle O \rangle}{\partial p}$ [21], (ii) $(N_{\text{spins}} - pV) \sim V^{1/2}$, which justifies the Taylor expansion $\frac{1}{N_{\text{spins}}} = \frac{1}{pV + (N_{\text{spins}} - pV)} = \frac{1}{pV} \left(1 - \frac{N_{\text{spins}} - pV}{pV} + \dots \right)$ and (iii) the finite-size scaling relation $\overline{\langle O \rangle} = L^{x_O/\nu} \mathcal{F}_O(L^{1/\nu}(p-0.8))$ holds when one works precisely at the critical temperature for $p=0.8$ (x_O is the scaling dimension for O).

susceptibilities. Indeed, our 12 real replicas are to remain statistically independent at all times. Hence, we cannot start a single-cluster update from the same site \mathbf{x} in all replicas. Here, we separate our simulations into two different phases:

- (i) During the update phase, we choose independently the starting site \mathbf{x} for the single-cluster update of each replica. The spin-configuration is updated after the cluster is traced.
- (ii) During the measuring phase, instead, the starting point for the cluster tracing is the same for all replicas. However, the spin configurations of the replicas are *not* modified after the $M_{\mathbf{x}}^{(q)}$ estimators are computed.

In both phases, the starting site for cluster tracing is chosen to be occupied (namely, $\epsilon_{\mathbf{x}} = 1$).

2.4.2. The computation of $\tilde{\chi}_q$. Our computation of the local susceptibilities $\tilde{\chi}_q$ employs 16 real replicas. The separation between the update phase and the measuring phase, which we have discussed above also applies to this case.

During the measuring phase, we compute for each replica:

$$N_{\mathbf{x}}^{(a)} = \sum_{\mathbf{y}} \gamma_{\mathbf{y},\mathbf{x}}^{(a)}. \quad (21)$$

We proceed by selecting a subset of q distinct replica indices a_1, a_2, \dots, a_q , and compute the estimator:

$$Y_{\mathbf{x},q} = \prod_{j=1}^q N_{\mathbf{x}}^{(a_j)}, \quad (22)$$

which has the thermal expectation value:

$$\langle Y_{\mathbf{x},q} \rangle = \chi_{\mathbf{x}}^q, \quad (23)$$

where the local susceptibility $\chi_{\mathbf{x}}$ is defined in equation (11). Of course, one may average over different choices of a subset of q distinct replicas in order to increase the statistics.

As in the previous section, we choose just one starting point \mathbf{x} during the measuring phase, with uniform probability $1/N_{\text{spins}}$. Hence,

$$\tilde{\chi}_q \approx \overline{\langle Y_{\mathbf{x},q} \rangle}. \quad (24)$$

The above equation is not an equality due to the fluctuations on the number of spins N_{spins} .

2.4.3. The computation of $C_q(r)$. As opposed to the strategy we have followed in the computation of the susceptibilities based on the simulation of a high number of replicas (in the same realization of the disorder), in the computation of the correlation function C_q we have chosen to simulate only one replica. This greatly simplifies the simulation but induces strong bias in the statistical estimator of C_q . In particular, it is possible to

Table 1. Details of our numerical simulations. We report the number of samples (disorder realizations), N_S , used in the different runs (χ_q susceptibilities, $\tilde{\chi}_q$ local susceptibilities and correlation functions). We also report the number of sweeps (as defined in the text) used for thermalizing the different systems, N_{sweeps} . In the χ_q susceptibility runs we have simulated 12 replicas per sample while for computing the local susceptibilities we have simulated 16 replicas per sample. In the correlation (Corr.) runs we have simulated only one replica per sample.

L	N_S (χ_q)	N_S ($\tilde{\chi}_q$)	N_S (Corr.)	N_{sweeps}
8		110 592		16
12	98 304	108 902		32
16	98 304	109 666		32
24	98 304	109 428		64
32	81 920	796 367	5000	64
48	81 920	109 528	5030	128
64	81 920	84 774	9800	128
96	81 920	84 034		512
128	26 984	60 015		512

show [17] that this bias is proportional to $1/N_m$ (N_m being the number of measurements on a given sample), and problems arise when the magnitude of this bias is similar to the statistical error induced by the disorder (proportional to $1/\sqrt{N_S}$ (N_S is the number of disorder realizations, samples)).

To resolve this bias, we have followed the strategy introduced in [17]. Let us work on a given sample (i.e. fixed disorder) and at equilibrium. Our strategy consists, first, of computing the total average of a given observable O , denoted as $O^{(1)}$. Then, we use two halves of the Monte Carlo simulation and compute the average value of O in these two halves and compute their mean, denoted as $O^{(2)}$. Finally, we obtain the average of O on each quarter of the Monte Carlo history and compute their mean, obtaining $O^{(3)}$. Finally, the unbiased quadratic estimator is [17],

$$O^Q = \frac{8}{3}O^{(1)} - 2O^{(2)} + \frac{1}{3}O^{(3)}. \quad (25)$$

In table 1, we report the number of samples used in the different runs.

3. Numerical results

In this section, we present our numerical results regarding multiscaling by analyzing the behavior of the correlation functions and the global and local susceptibilities.

3.1. Correlation functions

To quantify the $\zeta(q)$ exponent we have analyzed the dependence of C_q on C_1 . In figure 1, we show the behavior of C_q as a function of C_1 for three different lattice sizes and three

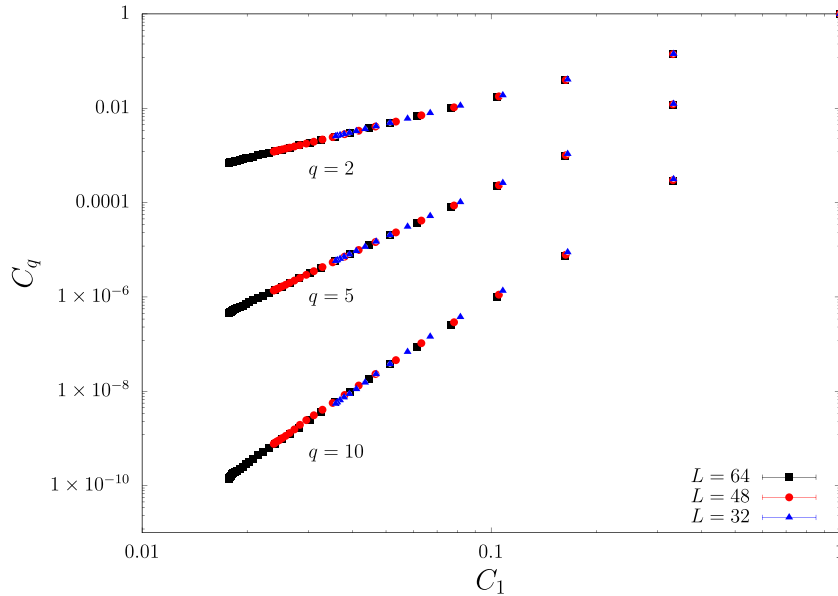


Figure 1. $C_q(r)$ versus $C_1(r)$ for $q=2, 5$ and 10 , and for $L=32$ (blue triangles), $L=48$ (red circles) and $L=64$ (black squares). Size of the error bars is smaller than those of the symbols.

values of q . The scaling of the data (for $L=32, 64$ and 128) is very good and the power-law dependence of C_q on C_1 is very clear and accurate.

In figure 2, we plot C_q/C_1^q as a function of C_1 in order to assess the multiscaling behavior. In all the simulated cases ($q \leq 10$) we have found diverging behavior as $C_1 \rightarrow 0$, which marks the onset of multiscaling behavior in this model. Note again the good scaling of the data from different lattice sizes ($L=32, 48$ and 64).

We estimate the $\zeta(q)$ exponent by fitting the correlation function data to equation (6). We fit $C_q(r)$ computed on a given lattice size against $C_1(r)$ computed on the same lattice size. We have computed the error bars of $\zeta(q)$ using the jackknife method over the number of samples, following the method of [22]. We perform independent fits on all the jackknife blocks using the diagonal covariance matrix, and then, the error bars in the parameters of the fit can be computed from the fluctuations among all the jackknife blocks.

We report our results in table 2. The exponent $\zeta(q)$ is not proportional to q . This clearly shows that the 3D diluted Ising model presents multiscaling behavior. Despite the fact that we are using a quasi-perfect action, we observe a small dependence of $\zeta(q)$ on the lattice size.

3.2. Global susceptibilities

Figure 3 shows the behavior of the χ_q susceptibilities as a function of the lattice size.

By fitting the susceptibilities presented in figure 3 we have estimated the $\tau(q)$ exponents using equation (8). The numerical estimates for the $\tau(q)$ exponents (and consequently those for the $\zeta(q)$ exponents) can be found in table 3.

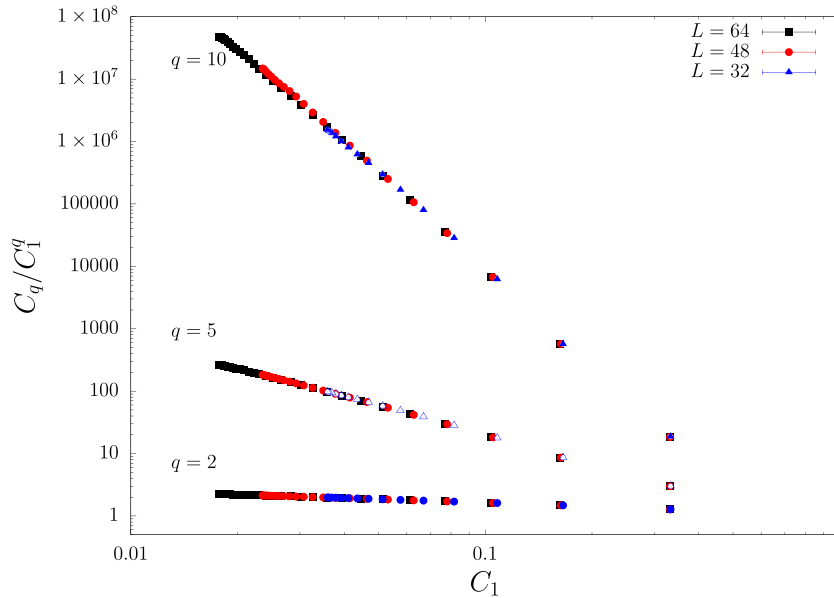


Figure 2. $C_q(r)/C_1^q(r)$ versus $C_1(r)$ for $q=2, 5$ and 10 , and for $L=32$ (blue triangles), $L=48$ (red circles) and $L=64$ (black squares). Note the potential growth in all the cases, which is a clear signal of the multiscaling behavior. All the curves take the value 1 as $C_1 = 1$ (the rightmost point of the plot). Error bars of the ratio have been computed using the jackknife method. Size of the error bars is smaller than those of the symbols.

Table 2. Exponent $\zeta(q)$ computed using the $L=32, L=48$ and $L=64$ correlation functions. This exponent has been computed using the jackknife method to address the high correlation of the data (different r in the correlations $C_q(r)$). We also report the C_1 interval used in the fits, (C_1^m, C_1^M) .

q	$L=64$		$L=48$		$L=32$	
	(C_1^m, C_1^M)	$\zeta(q)$	(C_1^m, C_1^M)	$\zeta(q)$	(C_1^m, C_1^M)	$\zeta(q)$
2	(0,0.3)	1.8109(3)	(0,0.3)	1.8094(7)	(0,0.3)	1.808(1)
3	(0,0.17)	2.457(1)	(0,0.3)	2.4525(19)	(0,0.3)	2.447(3)
4	(0,0.1)	3.026(4)	(0,0.16)	2.997(6)	(0,0.3)	2.993(8)
5	(0,0.1)	3.486(7)	(0,0.1)	3.474(13)	(0,0.3)	3.432(12)
6	(0,0.1)	3.849(9)	(0,0.1)	3.836(18)	(0,0.3)	3.803(18)
7	(0,0.1)	4.192(13)	(0,0.1)	4.17(2)	(0,0.3)	4.23(3)
8	(0,0.1)	4.483(17)	(0,0.1)	4.45(3)	(0,0.3)	4.54(5)
9	(0,0.1)	4.75(2)	(0,0.1)	4.72(4)	(0,0.3)	4.83(6)
10	(0,0.1)	5.00(3)	(0,0.1)	4.95(5)	(0,0.3)	5.10(7)

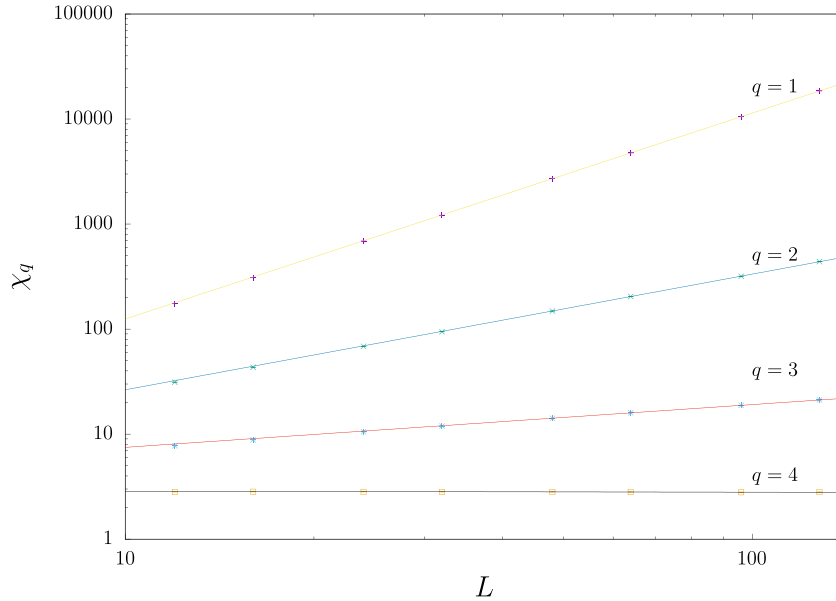


Figure 3. χ_q versus L for $q = 1, 2, 3$ and 4 in double logarithmic scale. Straight lines are fits to equation (8) using $L \geq 48$ to avoid the small scaling corrections. For $q \geq 4$, χ_q does not diverge, so $\tau(q) \geq D = 3$. In order to compute $\zeta(q)$ we have rescaled $\tau(q)$ using the numerical value for $1 + \eta = 1.036(1)$ (see equation (4)). Thus, $\zeta(q) = \tau(q)/(1 + \eta) = \tau(q)/1.036(1)$.

Table 3. $\tau(q)$ and $\zeta(q)$ exponents from the finite size scaling of the susceptibilities χ_q . For χ_4 , we do not detect divergence with L . Thus, for $q \geq 4$, $\tau(q) \geq 3$ and $\theta(q) \geq 2.89(1)$. We have computed, as a test, the $1 + \eta$ exponent in the $q = 1$ row, and it compares very well with the most accurate available estimate $1 + \eta = 1.036(1)$ [19].

q	$\tau(q)$	$\zeta(q)$
1	1.039(2)	1 (by def.)
2	1.893(3)	1.833(5)
3	2.586(4)	2.503(6)
4	≥ 3	$\geq 2.896(3)$

3.3. Local susceptibilities

In figure 4, we show the behavior of $R_q^{(1)}$ versus L for three different values of q , showing the power-law divergence implied by equation (12).

In table 4, we present our final values for the ζ -exponents and the (discrete) first and second derivatives obtained analyzing the observables $R_q^{(1)}$, $R_q^{(2)}$ and $R_q^{(3)}$, computing their error bars with the bootstrap method, and using only the lattice sizes with $L \geq 48$ (as for the global susceptibility analysis) to avoid small scaling corrections⁵. We plot our

⁵ An analysis using all the sizes and assuming the leading scaling correction term gives essentially the same exponents.

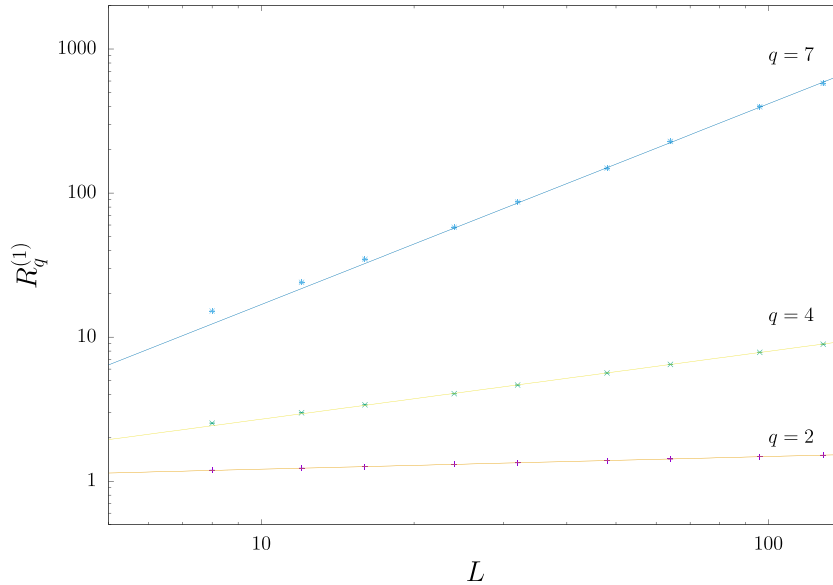


Figure 4. $R_q^{(1)}$ versus L for $q=2, 4$ and 7 in double logarithmic scale. Straight lines are fits to equation (12) considering scaling corrections. Error bars of all three ratios $R_q^{(i)}$ have been computed using the bootstrap method.

Table 4. $\zeta(q)$ exponents and the (discrete) first and second derivatives from the finite size scaling of the ratios $R_q^{(1)}$, $R_q^{(2)}$ and $R_q^{(3)}$ of the local susceptibilities $\tilde{\chi}_q$. Note that $\zeta(1) = 1$.

q	$\zeta(q)$	$\zeta(q) - \zeta(q - 1)$	$\zeta(q) + \zeta(q - 2) - 2\zeta(q - 1)$
2	1.830(2)	0.830(2)	
3	2.517(5)	0.688(3)	-0.143(2)
4	3.09(1)	0.573(6)	-0.115(3)
5	3.57(2)	0.481(9)	-0.092(4)
6	3.98(3)	0.40(1)	-0.077(6)
7	4.31(5)	0.33(2)	-0.07(1)
8	4.56(8)	0.25(4)	-0.08(2)
9	4.7(1)	0.16(6)	-0.09(2)
10	4.7(2)	0.05(9)	-0.10(3)

results for $\zeta(q)$ in figure 5 where the strong departure from the linear regime is clear, providing strong indications of multifractal behavior.

Furthermore, the results reported in table 4 show that the function $\zeta(q)$ is a non-decreasing function for the simulated values of q . In addition, it is a concave function of q , in agreement with the results from Ludwig [5] (see also A.2).

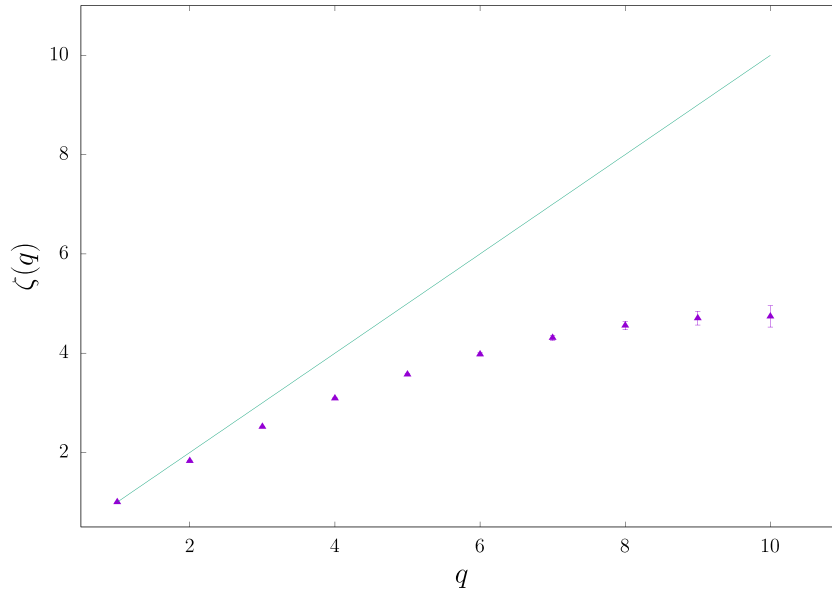


Figure 5. Exponent $\zeta(q)$ versus q (see results of table 4). By definition $\zeta(1) = 1$. We have also plotted the line $\zeta = q$ to show the appearance of the multifractal behavior in the model ($\zeta(q) \neq q$).

4. Discussion and conclusion

Over the years, many disordered ferromagnetic systems in 2D have been shown to exhibit multiscaling behavior (see e.g. [5]), with the surprising exception of the DIM. This is, however, marginal behavior. The DIM is the $Q = 2$ instance of the diluted Potts model with Q states (which does display multiscaling for $Q > 2$). Furthermore, it suffices to consider long-range interactions to find multiscaling in the 2D DIM (see [23] and references therein). The behavior of the DIM (with short-range interactions) in $D = 2$ is marginal in a different way, as well. Although there is no multiscaling in $D = 2$, in a pioneering work, Davis and Cardy [15] found multifractality in the DIM in space dimensions $D = 2 + \epsilon$. Here, we have extended Davis and Cardy’s [15] result to $D = 3$ through extensive numerical simulations for the site-diluted Ising model, which is studied under equilibrium conditions.

We have computed the exponents $\tau(q)$ for integer values $q = 1, 2, \dots, 10$. The q th power of the correlation function, equation (2), decays at long distances as $1/r^{\tau(q)}$ (3). We have found very clear numerical evidence for $\tau(q) < q\tau(1)$ for $q > 1$, which is the hallmark of multifractality.

Let us emphasize that multiscaling in no way contradicts the general Renormalization Group expectation of a universal large- L limit for relative cumulants of the order-parameter [24]. Specifically, for the very same model studied here, it was shown long ago that the relative variance of the squared order-parameter,

$$g_2 = \frac{\overline{\langle \mathcal{M}^2 \rangle^2} - \langle \mathcal{M}^2 \rangle^2}{\langle \mathcal{M}^2 \rangle^2} \quad \text{with} \quad \mathcal{M} = \sum_x \epsilon_x s_x, \quad (26)$$

reaches its expected universal limit [18] (this behavior is sometimes called no self-averaging [24]). One might think that having a finite large- L limit for g_2 somehow contradicts multiscaling. The correct conclusion is indeed different, as we now explain starting from the results discussed in appendix A.1. Consider the second moment, $q = 2$, which is one relevant in the computation of g_2 . The key point regards the spatial sites one integrates over:

- If one integrates $\overline{\epsilon_x \epsilon_y \langle S_x S_y \rangle^2}$ over \mathbf{y} the global susceptibility $\chi_{q=2}$ is obtained and the full multifractal signal is recovered.
- If one integrates instead $\overline{\epsilon_x \epsilon_{\mathbf{y}_1} \epsilon_{\mathbf{y}_2} \langle S_x S_{\mathbf{y}_1} \rangle \langle S_x S_{\mathbf{y}_2} \rangle}$ over \mathbf{y}_1 and \mathbf{y}_2 the resulting quantity is the local susceptibility $\tilde{\chi}_{q=2}$, which has only half the multifractal signal⁶.
- Yet, the required quantity in the computation of g_2 is $\overline{\langle \mathcal{M}^2 \rangle^2}$. Hence, we are able to integrate $\overline{\epsilon_{\mathbf{x}_1} \epsilon_{\mathbf{x}_2} \epsilon_{\mathbf{y}_1} \epsilon_{\mathbf{y}_2} \langle S_{\mathbf{x}_1} S_{\mathbf{y}_1} \rangle \langle S_{\mathbf{x}_2} S_{\mathbf{y}_2} \rangle}$ over \mathbf{x}_1 , \mathbf{x}_2 , \mathbf{y}_1 and \mathbf{y}_2 . However, integrals over \mathbf{x}_2 , \mathbf{y}_1 and \mathbf{y}_2 already suffice to completely suppress multifractal scaling. In fact, neglecting scaling corrections, $\overline{\langle \mathcal{M}^2 \rangle^2}$ scales with L in the same way that $\overline{\langle \mathcal{M}^2 \rangle}$ does.

In summary, the extreme self-averaging violations evinced by the multiscaling analysis can only be identified when studying correlations at the *local* level. Carrying out too many spatial integrations erases the multifractal signal. To unearth multiscaling, we have pursued here the same local approach that has been used in [13] in the context of the out-of-equilibrium dynamics of spin-glasses⁷.

Acknowledgments

We are grateful to Marco Picco for useful discussions and Maria Chiara Angelini for discussions about a related problem in the context of site percolation.

We thank the staff of the *Instituto de Computación Científica Avanzada de Extremadura* (ICCAEx), at Badajoz, where our simulations were carried out. This study was partially supported by Ministerio de Ciencia, Innovación y Universidades (Spain), Agencia Estatal de Investigación (AEI, Spain, 10.13 039/50 110 0011 033), the European Regional Development Fund (ERDF, A way of making Europe) through Grant Nos. PID2020-11 2936GB-I00 and PID2022-13 6374NB-C21, by the Junta de Extremadura (Spain) and Fondo Europeo de Desarrollo Regional (FEDER, EU) through Grant No. IB20079. This research has also been supported by the European Research Council under the European Unions Horizon 2020 research and innovation program (Grant No. 694 925-Lotglassy, G Parisi) and by ICSC-Centro Nazionale di Ricerca in High Performance Computing, Big Data, and Quantum Computing funded by the European Union-NextGenerationEU. E M acknowledges funding from the PRIN funding scheme (2022LMHTET—Complexity, disorder and fluctuations: spin glass physics and beyond)

⁶ $\tilde{\chi}_q$ more than compensates this disadvantage by scaling as a positive power of L for all $q \geq 1$.

⁷ However, it is worth recalling that the spin-glass criticality is much less understood due to the lack of a proper and easy-to-use renormalization group theory [25–27].

and from the FIS (Fondo Italiano per la Scienza) funding scheme (FIS783 - SMaC—Statistical Mechanics and Complexity: theory meets experiments in spin glasses and neural networks) from the Italian MUR (Ministry of University and Research).

Appendix. Some theoretical results

A.1. Scaling dimensions

In the replicated theory the C_q correlation functions can be written as,

$$\langle (\phi^{a_1}(\mathbf{x}) \cdots \phi^{a_q}(\mathbf{x})) (\phi^{a_1}(\mathbf{y}) \cdots \phi^{a_q}(\mathbf{y})) \rangle, \quad (\text{A.1})$$

with $1 \leq a_i < a_j \leq n$ for $i < j$, where $\phi^a(\mathbf{x})$ are the replicated fields with scaling dimension $[(D-2+\eta)/2]$ and n is the number of replicas ($n \rightarrow 0$).

As discussed in [5], the composite operator $(\phi^{a_1}(\mathbf{x}) \cdots \phi^{a_q}(\mathbf{x}))$ transforms following a reducible representation of the symmetric group (S_n) and, therefore, it is not a scaling operator at the random critical point. However, it can be expressed as a linear combination of scaling fields $\Phi_q^{\mu,\alpha}(\mathbf{x})$, and they each transform following the μ -irreducible representation (irrep) of S_n (α labels the multiplicity of the μ -irrep) [5], with scaling dimension $X_q^{\mu,\alpha}$. Its asymptotic behavior is,

$$\langle \Phi_q^{\mu,\alpha}(\mathbf{x}) \Phi_q^{\mu,\alpha}(0) \rangle \sim \frac{1}{|\mathbf{x}|^{2X_q^{\mu,\alpha}}}. \quad (\text{A.2})$$

Therefore, the behavior of C_q will be the sum (over the irreducible representations) of decays with powers $1/|\mathbf{x}|^{2X_q^{\mu,\alpha}}$, and the smallest scaling dimension $X_q^{\mu,\alpha}$ will determine its large scale behavior.

It is possible to show that for the spin operator (which is our case), all the different representations become degenerate as opposed to the energy operator [5, 15]. Therefore, $[(D-2+\eta)/2]\zeta(q)$ is the scaling dimension of the *full* composite operator $(\phi^{a_1}(\mathbf{x}) \cdots \phi^{a_q}(\mathbf{x}))$, which defines $\zeta(q)$ in such a way that $\zeta(1) = 1$.

Hence, the scaling behavior of C_q will be twice that of the composite operator $(\phi^1(\mathbf{x}) \cdots \phi^q(\mathbf{x}))$, namely $[(D-2+\eta)/2]\zeta(q) \times 2$.

In the case of the local susceptibilities $\tilde{\chi}_q$ we need to compute,

$$\frac{1}{V} \sum_{\mathbf{x}} \sum_{\mathbf{y}_1} \cdots \sum_{\mathbf{y}_q} \overline{\langle S_{\mathbf{x}} S_{\mathbf{y}_1} \rangle \cdots \langle S_{\mathbf{x}} S_{\mathbf{y}_q} \rangle}, \quad (\text{A.3})$$

so that in terms of the replicated theory, the associated correlation function can be written as,

$$\langle (\phi^{a_1}(\mathbf{x}) \cdots \phi^{a_q}(\mathbf{x})) \phi^{a_1}(\mathbf{y}_1) \cdots \phi^{a_q}(\mathbf{y}_q) \rangle, \quad (\text{A.4})$$

and the scaling dimension of the only composite operator $(\phi^{a_1}(\mathbf{x}) \cdots \phi^{a_q}(\mathbf{x}))$, is again $[(D-2+\eta)/2]\zeta(q)$ and each of the q -factors $\phi^a(\mathbf{y}_a)$ have $(D-2+\eta)/2$ as their scaling dimension.

Note that a field ϕ with $\dim(\phi)$ as the scaling dimension transforms following the rule $\phi(b\mathbf{x}) = b^{-\dim(\phi)}\phi(\mathbf{x})$.

Equation (A.3) can be written in the continuum as,

$$\tilde{\chi}_q \sim \frac{1}{L^D} \int d^D x \int d^D y_1 \cdots \int d^D y_q \langle (\phi^{a_1}(\mathbf{x}) \cdots \phi^{a_q}(\mathbf{x})) \phi^{a_1}(\mathbf{y}_1) \cdots \phi^{a_q}(\mathbf{y}_q) \rangle,$$

where the $q+1$ integrals run in the volume $[a, L]^D$ (a is the lattice spacing). After the change of variables $\tilde{\mathbf{x}} = \mathbf{x}/L$ and $\tilde{\mathbf{y}}_i = \mathbf{y}_i/L$ ($i = 1, \dots, q$) we can write:

$$\begin{aligned} \tilde{\chi}_q &\sim \frac{1}{L^D} L^{(q+1)D} \frac{1}{L^{((D-2+\eta)/2)\zeta(q)}} \frac{1}{L^{((D-2+\eta)/2)q}} \\ &\quad \times \int d^D \tilde{\mathbf{x}} \int d^D \tilde{\mathbf{y}}_1 \cdots \int d^D \tilde{\mathbf{y}}_q (\phi^{a_1}(\tilde{\mathbf{x}}) \cdots \phi^{a_q}(\tilde{\mathbf{x}})) \phi^{a_1}(\tilde{\mathbf{y}}_1) \cdots \phi^{a_q}(\tilde{\mathbf{y}}_q) \\ &\sim L^{(qD - [(D-2+\eta)/2](\zeta(q)+q))}, \end{aligned}$$

since the $q+1$ integrals in the tilde variables provided a constant in the large L -limit. Their integration limits are constrained to the volume $[a/L, 1]^D$, which is $[0, 1]^D$ for large L .

Taking into account this result, it is easy to obtain the behavior given in equations (12)–(14).

A.2. Concavity of the scaling exponents

Ludwig showed that $X_q^{\mu, \alpha}$ is a concave function⁸ of q [5]. The argument is simple, so we reproduce here for $\zeta(q)$. Note that if, for a given r , the correlation function for a given sample can take only values in the compact interval $[0, 1]$, then its probability density function (over the samples) is determined by its (q th) positive moments, which we have denoted as C_q . Moreover, these moments are smooth functions of q . Therefore, the $\zeta(q)$ exponents can also be defined for real q . In addition, $C_q^{1/q}$ is a non-decreasing function of q , which implies that $\zeta(q)$ is a concave function since $\zeta(q_1)/q_1 \leq \zeta(q_2)/q_2$ as $0 < q_2 < q_1$.

A.3. Davis–Cardy’s result

In [15], Davis and Cardy computed the scaling exponents $X_q^{\mu, \alpha}$ for the DIM in $2 + \epsilon$ dimensions. In the notation used in this paper, their result can be written as,

$$q - \zeta(q) = \left(\frac{q(q-1)}{2} \right) y + O(y^2), \quad (\text{A.5})$$

where y is the RG eigenvalue of the disorder strength, which is, at this order, $y = \alpha = O(\epsilon)$ (α is the specific heat exponent of the pure model and $\epsilon = D - 2$). These results clearly show that the DIM in $2 + \epsilon$ is expected to undergo multiscaling behavior.

⁸ To fix the notation, a concave function in an interval $[a, b]$ satisfies $f(\lambda x_1 + (1 - \lambda)x_2) \geq \lambda f(x_1) + (1 - \lambda)f(x_2)$ for $\lambda \in (0, 1)$ and for any two points x_1 and x_2 in the interval $[a, b]$.

However, in order to have an accurate analytical estimate of the difference $q - \zeta(q)$ for the 3D model one would need to extend this computation to higher orders of y [2].

References

- [1] Harris A B 1974 *J. Phys. C: Solid State Phys.* **7** 1671
- [2] Cardy J 1996 *Scaling and Renormalization in Statistical Field Theory (Lecture Notes in Physics vol 5)* ed P Goddard and J Yeomans (Cambridge University Press)
- [3] Harte D 2001 *Multifractals. Theory and Applications* 1st edn (Chapman and Hall/CRC)
- [4] Barabási A L and Stanley H E 2009 *Fractal Concepts in Surface Growth* (Cambridge University Press)
- [5] Ludwig A W W 1990 *Nucl. Phys. B* **330** 639–80
- [6] Dotsenko V, Dotsenko V and Picco M 1998 *Nucl. Phys. B* **520** 633–74
- [7] Lewis M A 1998 *Europhys. Lett.* **43** 189
- [8] Palágyi G, Chatelain C, Berche B and Igloi F 2000 *Eur. Phys. J. B* **13** 357 (available at: <https://link.springer.com/article/10.1007/s100510050042>)
- [9] Chatelain C, Berche B and Shchur L N 2001 *J. Phys. A: Math. Gen.* **34** 9593
- [10] Berche B and Chatelain C 2004 *Phase Transitions in Two-dimensional Random Potts Models* vol 4, ed Y Holovatch (World Scientific) p 146
- [11] Monthus C, Berche B and Chatelain C 2009 *J. Stat. Mech.* **12002**
- [12] Evers F and Mirlin A D 2008 *Rev. Mod. Phys.* **80** 1355–417
- [13] Baity-Jesi M *et al* 2023 (arXiv:2306.04591)
- [14] Cardy J 1999 (arXiv:cond-mat/9911024v1)
- [15] Davis T and Cardy J 2000 *Nucl. Phys. B* **570** 713–25
- [16] Wolff U 1989 *Phys. Rev. Lett.* **62** 361–4
- [17] Ballesteros H G, Fernandez L A, Martín-Mayor V, Muñoz Sudupe A, Parisi G and Ruiz-Lorenzo J J 1998 *Nucl. Phys. B* **512** 681
- [18] Ballesteros H G, Fernandez L A, Martín-Mayor V, Muñoz Sudupe A, Parisi G and Ruiz-Lorenzo J J 1998 *Phys. Rev. B* **58** 2740
- [19] Hasenbusch M, Toldin F P, Pelissetto A and Vicari E 2007 *J. Stat. Mech.* **02016**
- [20] Sokal A D 1997 Monte Carlo methods in statistical mechanics: Foundations and new algorithms *Functional Integration: Basics and Applications (1996 Cargèse School)* ed C DeWitt-Morette, P Cartier and A Folacci (Plenum)
- [21] Ballesteros H G, Fernández L A, Martín-Mayor V, Muñoz-Sudupe A, Parisi G and Ruiz-Lorenzo J J 1997 *Phys. Lett. B* **400** 346–51
- [22] Yllanes D 2011 Rugged free-energy landscapes in disordered spin systems *PhD Thesis* Universidad Complutense de Madrid (arXiv:1111.0266)
- [23] Chippari F, Picco M and Santachiara R 2023 *J. Stat. Mech.* **043301**
- [24] Aharony A and Harris A B 1996 *Phys. Rev. Lett.* **77** 3700–3
- [25] Angelini M C, Parisi G and Ricci-Tersenghi F 2013 *Phys. Rev. B* **87** 134201
- [26] Angelini M C and Biroli G 2017 *J. Stat. Phys.* **167** 476–98
- [27] Lubensky T, Temesvári T, Kondor I and Angelini M C 2023 Renormalization group in spin glasses *Spin Glass Theory and Far Beyond: Replica Symmetry Breaking After 40 Years* (World Scientific) pp 45–67